Online Impedance Measurement of Batteries Using the Cross-Correlation Technique

Taha Nurettin Gücin and Levent Ovacik

***Abstract*—Electrochemical impedance spectroscopy (EIS) is a powerful test technique that is extensively applied to electrochemical cells for determining the frequency response of the cell impedance. The results from EIS may be used for many applications, such as state of charge (SOC) and state of health. This article presents an approach for online EIS based on cross-correlation technique applied to a boost-type dc–dc charge controller for batteries. The theoretical background is explained and some improvements specific to battery applications are suggested. Preparation of noise datasets, postprocessing of results, and model fitting of the measurements are discussed in detail. The validity of the approach is experimentally confirmed with a digitally controlled boost converter that is charging a 12-V, 7-Ah sealed lead-acid battery: First, the perturbation magnitude is determined experimentally and then the battery is tested via the proposed method at 50% SOC. It is shown that the results of the present approach coincide with those obtained by a commercially available, laboratory-type, high-precision instruments. Finally, the tests were also repeated for 25% and 75% SOC values. It is shown that the proposed approach can be reliably used to analyze the impedance of batteries over a wide frequency range during battery charging process.**

***Index Terms*—Battery, cross-correlation, dc–dc converter, electrochemical impedance spectroscopy (EIS), impedance analyzer, state of charge (SOC), state of health (SOH).**

I. Introduction

THE process of obtaining complex valued impedance diagrams of electrochemical devices, such as the batteries, is generally referred as electrochemical impedance spectroscopy (EIS). In the recent literature, there are numerous studies reporting that essential information, such as the state of charge (SOC), the state of heath (SOH), and even internal temperature of various type of batteries can be estimated by careful interpretation of these diagrams [1]–[10].

The EIS provides the complex impedance information over a certain frequency range. In fact, most of the valuable information about the characteristics of batteries generally appears in the low-frequency region. Depending on the battery type, the frequency of range of interest generally resides in between a few mHz to a few hundred Hz. Furthermore, very accurate measurements are needed since the impedance values at low-frequency region are generally in a few milliohm values. Although there are commercially available EIS devices that are capable of providing very accurate measurements ranging from μHz to MHz frequency range, they are generally very expensive and therefore not suitable for online applications. On the other hand, in online application, it is generally desired to measure specific battery parameters, such as SOC and SOH, without the necessity of disconnecting the test device and interrupting the operation of the power system to which the battery is connected. The paper [11] presents how online EIS measurements can be utilized for battery status monitoring. Using the obtained EIS results and extreme learning machine ELM, they present how SOC of batteries during constant current and constant voltage charging operation can be measured [11].

Unfortunately, in obtaining EIS measurements online, conventional laboratory type instrumentation significantly limit the spread use of this test technique. A special measurement hardware has to be developed and integrated into the existing system.

Due to these reasons, there is a special interest for building cost effective EIS systems using commercially available components [12]. The study [12] compares nonsinusoidal excitation of the battery currents with regards to the suitability to the EIS. Moreover, a practical online EIS system consisting of commercial components, such as battery charger/discharger, power controller, and data acquisition system, has been set up for performing EIS measurements on a kilowatt-class battery system. In this article, periodic square, triangular and sawtooth waveforms are investigated. It is concluded that the square wave current injection on battery is the most convenient option.

Furthermore, there are several studies in literature offering online EIS measurements of batteries. One of the preferred approaches is to excite the battery current with the help of an programmable electronic load and perform EIS with the resulting voltage and current waveforms. Such an approach has been presented in [13], where broadband impedance spectroscopy (BIS) that utilizes a signal composed of multiple sine waves and EIS, which is based on single frequency excitation, have been compared. The authors have also discussed the optimization of the multisine excitation signal and gives a brief summary to conventional battery tests. The proposed multisine signal is applied to the battery via an electronic load.

An alternative approach for online EIS systems is to integrate the EIS functionality into the power converter, which regulates the energy transfer within the battery system. One such study

Manuscript received June 26, 2019; accepted August 21, 2019. Date of publication September 2, 2020; date of current version January 10, 2020. This work was supported in part by Istanbul Technical University (ITU) as a Scientific Research Project with the Project-ID 39801. Recommended for publication by Associate Editor R. Zane. *(Corresponding author: Taha Nurettin Gücin.)*

The authors are with the Electrical Engineering Department, Istanbul Technical University, 34469 Istanbul, Turkey (e-mail: tngucin@gmail.com; levent.ovacik@gmail.com).

Color versions of one or more of the figures in this article are available online at http://ieeexplore.ieee.org.

Digital Object Identifier 10.1109/TPEL.2019.2939269

[14] intends to perform an online impedance spectroscopy for a sealed lead-acid (SLA) battery with the purpose of battery characterization. The impedance spectroscopy is achieved by altering the controller reference of the dc–dc converter to inject ac currents into battery charging current at varying frequencies. This procedure is repeated separately for each frequency. In this case values are between 0.32 and 1024 Hz. The test at 0.32 Hz approximately takes 15 s. The study successfully obtains the complex impedance at different SOCs of the battery [14].

Huang and Qahouq [15] obtains the impedance magnitude of a lithium-ion battery by injecting an ac duty cycle perturbation and measuring the current and voltage waveforms. The method uses the obtained information (the value of the charging current and dc–dc converter output voltage) to estimate the open circuit voltage (OCV) so that the SOC can be predicted. The study claims that the method can be applied to various battery types such as Li-ion, SLA, and nickel metal-hydride batteries.

A more recent study, [16], investigates a method for online battery impedance measurement for batteries. The study contains the measurement process by two different noise excitation sources. In the former case, the battery is excited by an electronic load, which is controlled by an external signal. In the latter case, the battery is excited by a motor controller and a brushless permanent magnet motor operating in current control mode. The complex impedance of the batteries are obtained by cross-correlation technique. The method was applied to two battery types, lithium-iron-phosphate (LFP) and nickel manganese cobalt oxide (NMC) batteries. Estimation of SOC for LFP batteries is found to be challenging, while it is stated that estimation is possible for NMC batteries.

Another EIS measurement application implemented for a bidirectional battery charger based on the half-bridge topology is presented in [17]. The study aims to provide a guideline for designing a precise controller that is able to excite the battery with a triangular current waveform, so that it is possible to identify the battery impedance by making use of fourier transforms.

Lee *et al.* [18] integrated an online impedance measurement system into a high power battery charger by injecting an ac current ripple on a dc charging current. The frequency of the injected ac current ripple is swept from 0.1 to 100 Hz. The impedance data are obtained by transferring the current and voltage signals into a stationary rotating coordinate system.

The study presented in [19] utilizes a bidirectional dc–dc converter for implementation of an online multisine BIS, where the duty cycle of the converter is perturbed with a signal that is summation of several sine waves at the frequencies of interest. The study discusses the design procedures for the perturbation signal.

This article intends to implement the cross-correlation method on digitally controlled dc–dc converters, since power systems containing batteries mostly include dc–dc converters for battery charging/discharging purposes. Thus, it is aimed to enable the dc–dc converters to perform online EIS measurements. The literature survey presented above reveals that the general approach of online battery impedance identification studies utilizing dc–dc converters is based on injecting a sinusoidal ac current with a specific frequency on the battery charging current and to identify the phase shift and impedance magnitude from the voltage and current waveforms. However, this method requires the applied ac current to be repeated for all frequencies of interest.

The cross-correlation-based identification procedure enables gathering information over a wide frequency range via single test, since all frequencies can be excited with a single test. The data range and resolution of the obtained results depend on sampling parameters and testing time [20]. Although cross-correlation-based identification technique has been applied for the dc–dc converter identification applications by several studies [21]–[24], there are only few studies implemented on dc–dc converters for identification of passive impedance networks [20] and network impedances [25]. The study presented herein is an improved application of cross-correlation technique for identification of battery impedances.

II. EIS of Batteries

There are various studies focusing on the analysis of battery complex impedances [1]–[9]. The earliest trials for battery impedance measurements are reported to be conducted in 1941 by E. Willihnganz, where an electrochemical battery cell was excited with a 5 mV amplitude ac signal [3]. Such tests allow the scientists to evaluate and extract some critical information concerning the battery dynamics and kinetics. Usually different set of information can be obtained by measurements at various frequencies. The process of obtaining the complex impedance for batteries are sometimes called the EIS.

The measurements are performed in either galvanostatic or potentiostatic mode. While the galvanostatic mode represents the case where a certain current is injected into the battery as the voltage is observed. Vice versa, in the potentiostatic mode a certain voltage is applied to the battery and the current is observed. The galvanostatic mode is usually preferred due to very low resistance values of the battery packs, so that the current is limited in this measurement mode.

As mentioned previously, EIS might be used for estimation of many important parameters and states of batteries. Generally speaking, the state estimation of batteries is performed by extraction of a single or multiple parameter/parameters of an equivalent electrical model of the battery under test.

A generic equivalent electrical model for an electrochemical cell can be expressed with inductive, resistive, and capacitive components. The resistive component, R_e, imitates the behavior of the electrolyte, current-collectors and bulk of the electrode materials. Moreover, it covers for electron-transfer reactions. The capacitive component, $(C_{DL}||R_{CT})$, is generally used to represent the behavior of double-layer capacitance. On the other hand, the inductive component, L_e, is included in the model to represent the porous nature of the electrodes. All of these components together represent the electrical equivalent circuit of a battery [3] shown in Fig. 1. Furthermore, Warburg Impedance as shown in Fig. 1, denoted by W, is also generally included in the model for simulating the low-frequency behavior of the

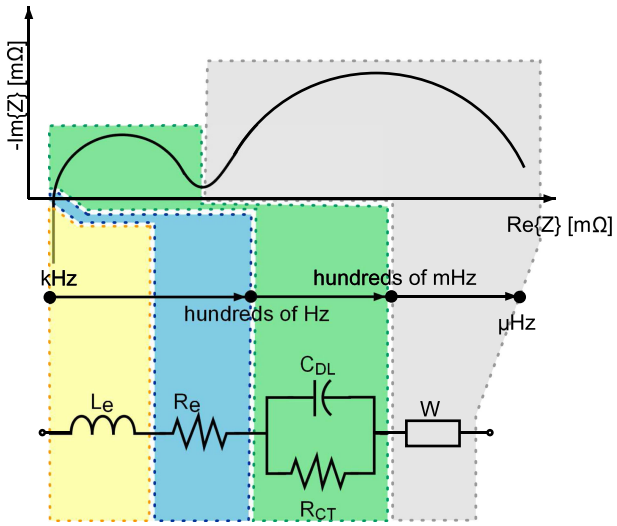

Fig. 1. General representation of the relationship of the battery equivalent circuit and the Nyquist diagrams.

battery. It should also be noted that, depending on the battery type, the Warburg Impedance might be represented by placing it in series with R_{CT} [7], [26].

A generic example for battery cell Nyquist diagram, where the impedance of the battery cell is represented in real (x-axis) and imaginary (y-axis) components, is also illustrated in Fig. 1. As it can be seen, the diagram consists of a vertical line at the beginning, followed by two semicircles. Corresponding frequency values are expressed in the figure. Clearly, in high-frequency region the inductance is dominant. The first semicircle usually corresponds to a frequency range of several hundred Hz to 10^{-1} Hz.

The Warburg Impedance, which corresponds to the second semicircle at Fig. 1, occurs due to diffusion mechanism in the battery and it is dominant in very low-frequency region, which is generally between μHz and mHz. On a Nyquist diagram, in the low-frequency zone, impedance might be observed in different shapes such as a semicircle, linear curve, etc. [2], [27]. Moreover, there are some studies that are utilizing constant phase elements (CPEs) characterized by $Z_{CPE} = \frac{1}{j\omega^n Q}$, instead of the capacitors [9], [28].

III. Cross-Correlation Method

This article utilizes the cross-correlation-based system identification method for obtaining the impedance of a battery cell/pack under test. A more comprehensive and detailed information about cross-correlation method might be found in [29], [30].

The output response of an linear time invariant (LTI) system, $y(t)$, is defined by the convolution of the applied signal, $x(t)$, and the impulse response of the system, $h(t)$, as follows:

$$y(t) = x(t) * h(t) = \int_{-\infty}^{\infty} x(\tau)h(t-\tau)d\tau. \tag{1}$$

For a sampled system, the output response, $y[n]$, of a system, $h[n]$, to the input signal, $u[n]$, can be formulated as

$$\begin{aligned} y[n] &= \sum_{k=-\infty}^{\infty} h[n-k]u[k] + v[n] \\ &= \sum_{k=-\infty}^{\infty} h[k]u[n-k] + v[n]. \end{aligned} \tag{2}$$

The unwanted disturbances, such as the noise, are presented as $v[n]$. The cross-correlation of input $u[n]$ and output $y[n]$ is defined as

$$r_{uy}[m] = \sum_{n=1}^{\infty} u[n]y[n+m] = \sum_{n=1}^{\infty} h[n]r_{uu}[m-n] + r_{uv}[m]. \tag{3}$$

Here, $r_{uu}[m]$ represents the autocorrelation of input signal, whereas the cross-correlation of input signal and disturbances are disturbances represented as $r_{uv}[m]$. These terms are mathematically defined as

$$r_{uu}[m] = \sum_{n=1}^{\infty} u[n]u[n+m] \tag{4}$$

$$r_{uv}[m] = \sum_{n=1}^{\infty} u[n]v[n+m]. \tag{5}$$

By taking the Fourier transform of (3), following equalities are derived:

$$R_{uy}(j\omega) = H(j\omega).R_{uu}(j\omega) + R_{uv}(j\omega) \tag{6}$$

$$H(j\omega) = \frac{R_{uy}(j\omega) - R_{uv}(j\omega)}{R_{uu}(j\omega)}. \tag{7}$$

When the input signal is white noise (WN), the autocorrelation and cross-correlation functions exhibit the following properties:

$$r_{uv}[m] = 0 \tag{8}$$

$$r_{uu}[m] = \sigma^2\delta[m] \tag{9}$$

where σ is the standard deviation of the input signal. Considering the mentioned properties, the (6) can be expressed as

$$H(j\omega) = \frac{R_{uy}(j\omega)}{R_{uu}(j\omega)} = \frac{R_{uy}(j\omega)}{\sigma^2}. \tag{10}$$

As shown above, the system transfer function is now represented in frequency domain as $H(j\omega)$, which will be used in the following section for deriving the impedance of a device under test (DUT), a battery in this case.

IV. Impedance Measurement by Cross-Correlation Technique

As mentioned previously, the cross-correlation technique is based on applying a WN-signal at the input of a system and observing the output of the system. For the intended use in this article, applying a WN as current/voltage to a battery and observing the voltage/current waveforms would be required. However, it may not be practical to build a circuit that could directly inject

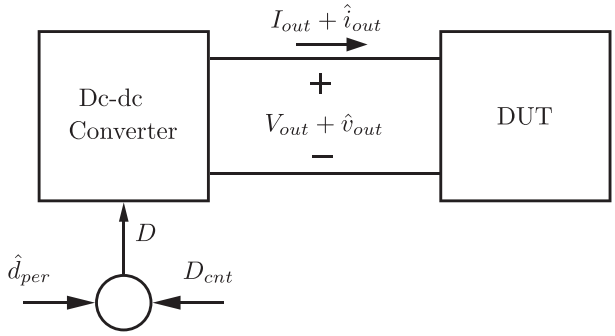

Fig. 2. Impedance measurement utilizing cross-correlation technique.

a WN-like current/voltage. A more practical way, as illustrated in Fig. 2, is to apply a pseudorandom noise perturbation signal, $\hat{d}_{\rm per}$, to the duty cycle command, $D_{\rm cnt}$, of a converter which results in a total duty cycle of D, so that both control to output voltage transfer function, $G_{vd}(s) = \frac{\hat{v}(s)}{\hat{d}(s)}$, and control to output current transfer function, $G_{id}(s) = \frac{\hat{i}(s)}{\hat{d}(s)}$, could be derived. As formulated below, the impedance of the load at the output of the dc–dc converter can be calculated by the division of these control transfer functions.

$$\frac{G_{vd}(s)}{G_{id}(s)} = \frac{\hat{v}(s)}{\hat{i}(s)} = Z(s). \tag{11}$$

In the ideal case, the input perturbation to duty cycle command is a WN signal, which exhibits previously mentioned properties. On the other hand, an ideal WN signal is impossible to derive. Many studies utilize pseudorandom-binary-sequence or other approximations. In this article, a random integer number WN approximation, which is added to the steady state duty cycle, is utilized for the intended application.

As mentioned previously, the cross-correlation technique excites all the frequencies in a single test, rather than testing the battery separately for each frequency. The upper limit, $f_{\rm stop}$, lower limit, $f_{\rm start}$, and resolution Δf of the obtained frequency spectrum depend on the sampling frequency, f_s and number of acquired data points, K. Same quantities may also be expressed in terms of perturbation frequency, $f_{\rm per}$ and length of perturbation signal, N, as follows:

$$f_{\rm start} = \frac{f_{\rm per}}{N} = \frac{f_s}{K} \tag{12}$$

$$f_{\rm stop} = \frac{f_s}{2} \tag{13}$$

$$\Delta f = \frac{f_{\rm per}}{N} = \frac{f_s}{K}. \tag{14}$$

One other critical parameter is the testing time of the DUT, which can be calculated as

$$T_{\rm test} = \frac{N}{f_0} = \frac{K}{f_s} = \frac{1}{f_{\rm start}}. \tag{15}$$

As it can be seen from equations above, the qualities of the EIS measurements by proposed approach depend on perturbation noise data length, perturbation frequency, or sampling total number of recorded data points and sampling rate.

V. Application of Cross-Correlation Technique for Batteries

Here, a couple of improvements for the method are proposed for the battery-specific impedance identification application. These suggestions aim to ensure better results concerning the dynamic behavior of the battery for EIS-oriented applications.

A. Performing Moving Average on Measured Battery Voltage Data

As mentioned previously, batteries are highly nonlinear and dynamic devices. The first major issue in an online application is the fact that battery OCV continues to increase as the battery is being charged while it is under test.

For the impedance identification of the batteries, it is intended to utilize the perturbation-caused voltage and current waveforms during the test. Thus, other effects on the voltage and current waveforms, such as the increase in the OCV, should be somehow eliminated since they are not related to the impedance of the battery.

The cutoff frequency of the moving average filter is equal to $f_{co} = f_s/M$, where M is the window size of the filter. Using this equation, the correct window size can be chosen with regards to the frequency range of interest.

Although it is one of the most common filters, performing moving averages on the test data and subtracting it from the test data would be an effective way to obtain the voltage and current waveforms that are related to the perturbation of the duty cycle, $\hat{d}_{\rm per}$.

In Fig. 3 the battery voltage data during a test (blue curve) and the calculated moving average (red curve) is illustrated. The calculated moving average is then subtracted from the original data, so that the result would be a good representative of the waveforms that are caused by the duty cycle perturbation for identification purpose, $\hat{d}_{\rm per}$.

B. Performing Two Separate Tests With Different Noise Colours

The literature survey shows that, most important parameters for applications such as SOC and SOH estimation generally reside in the low-frequency region. Thus, it is of great interest for researchers to obtain impedance variation in the low-frequency region more precisely.

Consequently, it is proposed to perform two separate tests specifically aimed for low- and high-frequency impedance information as a further improvement. For this purpose, a red noise (RN) signal, which has a higher power spectral density (PSD) in low-frequency, and a WN signal is injected separately into the duty cycle, $D_{\rm cnt}$. The PSDs of produced RN and WN are illustrated in Fig. 4. It should also be noted that, since the PSD of the RN injection is very low in higher frequencies, the high-frequency impedance information during this test would be highly attenuated by the dc–dc converter, which would then result in an invalid data in this region. Therefore, the data from two tests are processed separately and then merged into one final

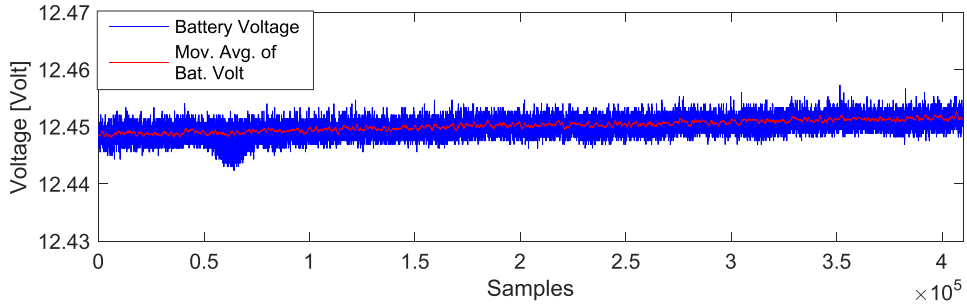

Fig. 3. Application of moving average on measured battery voltage.

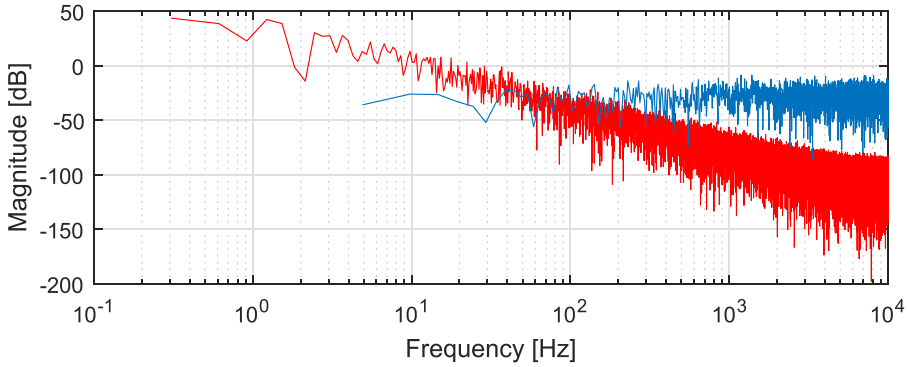

Fig. 4. Spectra comparison of applied perturbations for both tests.

dataset to have a clear representation of impedance information over a wide range of frequency.

The noise signals were prepared by using a set of random integers, which are added to the counter of the pulsewidth modulation (PWM) generator during the testing procedure. The magnitude of the designed noise data are limited to be less than 10% of the maximum duty cycle, to enable stability and linearity [19]. In fact, the noise is set to be $\pm 4\%$ of the maximum duty cycle. Furthermore, a scaling coefficient for the perturbation data are also implemented in field-programmable gate array (FPGA) so that the proposed system can be tested under different perturbation magnitudes.

For obtaining a RN dataset, the set of random integers is transferred to the frequency domain by taking the fourier transform. Afterward, it is multiplied by a desired slope, which in this case is -20 dB/dec, so that the signal is more powerful in the low-frequency region. After taking the inverse fourier transform, the dataset for RN signal is achieved.

As seen in Fig. 4, the intersection point of power spectral densities of two signals that are used in this article are around 100 Hz. Thus, the final data set is obtained by merging the RN injected test results up to 100 Hz and WN injected test results starting from 100 Hz.

VI. Postprocessing the Obtained Frequency Response Data

In real-world applications, some mechanisms, such as noise from switching and electromagnetic interference (EMI)/electromagnetic compatibility (EMC) issues, analog-to-digital converter (ADC) quantization process, and measurement errors, might distort the obtained results. Therefore, some data processing techniques are generally required to smooth out the obtained results. The background work for some of these techniques have already been presented in [20].

A. Performing Moving Averages

Application of moving averages on the obtained results is a basic, simple way to smooth the obtained impedance diagrams. However, it is advised to care for choosing a suitable window size.

Moreover, for avoiding filter lag and consequently a shift in the frequency of the obtained results introduced by this filter, it is suggested to utilize the zero-lag moving average. A zero-lag moving average can be obtained by calculating the moving average, MA_L of desired window size, L, and a second moving average, $MA_{L/2}$, with a window size of $L/2$ [31]. Then the zero lag moving average, MA_0 is equal to

$$MA_0 = MA_L - (MA_L - MA_{L/2}). \tag{16}$$

B. Median Filter

Another useful technique is the median filter that principally checks each data point whether or not it is representative of its surrounding data points. The median filter replaces data that are not representative of its neighbors with the median value. Application of this technique ensures a further improvement in

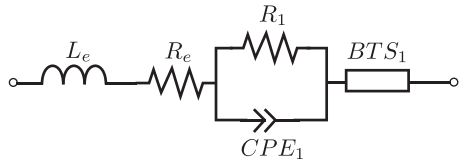

Fig. 5. Model used for curve fitting.

the processing of the obtained impedance data when a filter with a suitable window size is applied.

C. Fractional-Decade Processing

As mentioned in the explanations of previous techniques, choosing a reasonable window size is an important key to have affective results. To be able to smooth the obtained data, a reasonable window size should be determined concerning the number of data points and the frequency resolution. Clearly, a fixed window size over the complete frequency range should be avoided.

Consequently, it is suggested to choose different window sizes for each decade of the obtained impedance diagram which would assure better results. For the postprocessing of the results obtained in the framework of this article, the total number of data points in each decade is calculated. Afterward, for each decade one-hundredths and one-thousandths of these numbers are utilized as the window sizes for median filter and moving average filter, respectively.

D. Curve Fitting Based on an Equivalent Model

For further improvement, it is suggested to fit the obtained results also into an equivalent model. This way, it would be possible to clear the obtained results even further and enable more precise parameter estimation, on which a lot of EIS-based applications rely on.

The equivalent battery model should be chosen carefully, depending on the battery type, so that a high correlation between the obtained results and fitted model could be achieved.

The equivalent battery model, which is chosen for fitting the obtained data, is given in Fig. 5. In a recent study, Aksakal and Sisman [32] reports that the electric equivalent circuit model composed of inductance L_e, resistor R_e, Bisquert Short (BTS) elements Z_{BTS}, and constant phase elements CPE_1 in parallel with a resistor R_1 constituting $Z_{CPE||R}$, exhibits the best correlation between the measurements and the models for enhanced flooded lead-acid batteries. For the test frequency range of this article, it has been seen that one CPE and one BTS element was enough to model the battery, whereas [32] suggests to use two CPEs and two BTSs for modeling a wider frequency range.

The BTS model utilized here is generally used for modeling transmission lines [33]. Bisquert shows that it can be used for modeling electrochemical devices [34]. On the other hand, the CPE models are used for imitating the nonideal capacitor behavior, which appears as semicircles on Nyquist plots [32]. The equations for CPE with a parallel resistor are given below

$$Z_{CPE||R} = \frac{R}{1 + (j\omega)^{\alpha} QR}. \tag{17}$$

For the CPE models; the components R and Q are used for modeling the resistive and nonideal capacitive behavior to the order α, respectively. On the other hand, the BTS component is formulated as

$$Z_{BTS} = \sqrt{\zeta \cdot \chi}\, tanh\left(L_{BTS} \cdot \sqrt{\frac{\chi}{\zeta}}\right) \tag{18}$$

$$\zeta = \frac{r_{BTS}}{1 + (j\omega)^{\alpha_{BTS}} q_{BTS}.r_{BTS}} \tag{19}$$

where L_{BTS} is the depth of the pore within a porous electrode, χ is the impedance of the electrolyte within the pore, and ζ describes the impedance at the active interface region on the surface of the electrode. Please note that ζ is actually a CPE element that is implemented into the BTS component. For avoiding any confusion, the parameters of ζ is denoted as; r_{BTS}, q_{BTS}, and α_{BTS} instead of R, Q, and α, respectively.

VII. Experimental Setup

It has been decided to demonstrate the proposed method on a lead-acid battery, since they still have a huge share on the market, especially for stationary energy storage applications. Thus, aFPGA-based controller platform, Digilent Nexys 4 DDR, is utilized to control a boost converter-based battery charger for charging and testing a 12-V, 7-Ah Yuasa NP7-12 battery. The tests are performed while the battery was being charged with 0.35 A. The experimental setup and the schematic of the setup has been presented in Fig. 6. It was decided to use an FPGA-based controller platform, so that a specialized pulsewidth modulator could be designed in very high speed integrated circuit hardware description language for implementing the cross-correlation technique. The designed modulator is able to read a predefined noise data and apply this data as a perturbation on the actual duty cycle with an adjustable period at high precision. The noise data are produced in MATLAB and stored in the FPGA.

For identifying the battery impedance, it is necessary to measure and store the voltage and current waveforms of the battery. For this purpose a signal conditioning module was also designed, enabling the conditioning of the current and voltage waveforms to be logged by a data acquisition system, cDAQ of National Instruments (NI). For this purpose, a programmable-gain amplifier, THS7002, was used. This amplifier is able to have a gain of less or more than 1, so that it was used to amplify the current signal, whereas it was also able to decrease the magnitude of the battery voltage to fit in the ± 10 V input voltage range of the data acquisition system.

The voltage and current waveforms were stored by a data acquisition system composed of National Instruments (NI) cDAQ-9174 and NI 9222: a 4-channel, 16-b, 500 kS/s/ch simultaneously sampling voltage input module. The obtained data was captured by and postprocessed in MATLAB.

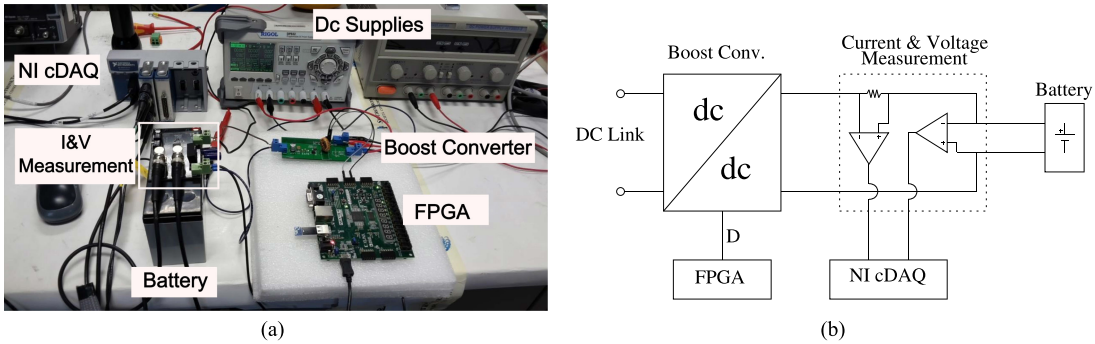

Fig. 6. (a) Experimental setup and (b) schematic of the setup.

The battery under test was conditioned for measurement according to the EN 50342-1 CENELEC standard: The battery was fully charged with a constant current of 1.75 A up to 14.8 V and then it was discharged with a constant current of 0.7 A for 2.5, 5, and 7.5 h so that the SOC was determined to be 75%, 50%, and 25%, respectively. The charging and discharging cycle was performed before each test and afterward the battery was left to a relaxation period until the variation of the open circuit battery voltage was less than 1 mV/min.

For checking the validity of the results, a reference measurement was made by a commercially available high precision impedance analyzer, a Gamry Reference 3000 system, at 50% SOC, between 10 mHz and 10 kHz. In the following figures, the results of the proposed technique are always presented in comparison with this reference measurement.

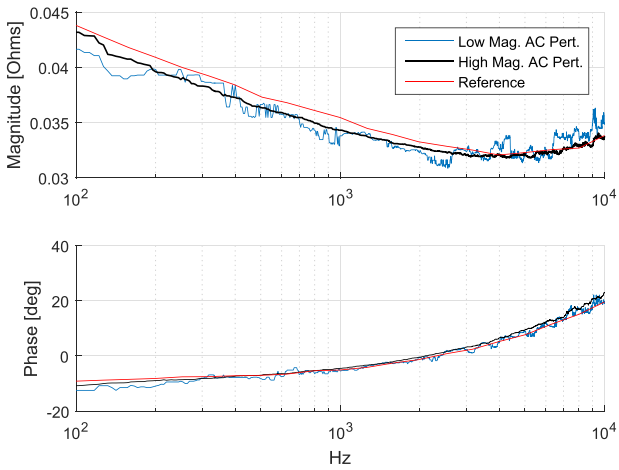

Fig. 7. Results of WN test for different noise excitation magnitude level, where blue and black curves have scaling factors of one and four, respectively.

VIII. Experimental Results

A. Determination of Noise Perturbation Magnitude

Previously, it has been explained how the noise magnitude was determined. However, if the perturbation magnitude is too small, then the data acquisition system might not be able to capture all the dynamics during the test, which in return would affect the analysis significantly. On the other hand, if the noise magnitude is too big, the linearity of the system might be jeopardized.

Thus, the choice of noise magnitude is a compromise between precision and system integrity. Consequently, it has been decided to perform tests with different noise magnitudes to find the better option.

For this purpose, the battery was analyzed by tests utilizing different WN magnitudes. As explained previously, a scaling factor that multiplies the WN signal was already implemented into the FPGA. In Fig. 7, the results for two WN tests with scaling factors of one and four, are presented.

For checking the measurement quality and displaying the difference of measurements with different perturbation magnitudes, it has been decided to perform Kramers–Kronig (KK) analysis, which is often used for EIS measurements. The KK-test provides a quick check for measurement quality and validity [35], [36]. It relies on the fact that the imaginary part of the impedance can be derived from real part and vice versa, given that the system is linear, time-invariant, and causal. The derived results are then compared with the measurements and the difference is presented as residual plots. The residual plots for both tests are illustrated in Fig. 8.

As it can be seen both from Figs. 7 and 8, the measurement with a scale factor of four has provided much more reliable results, whereas the measurement with scale factor one yielded noisy results. Thus, it has been decided to proceed further with the scaling factor of four.

The corresponding battery voltage- and current waveform magnitudes over the whole frequency bandwidth are also illustrated in Fig. 9. It can be seen that, the noise perturbation causes really small excitation, especially on the voltage. Therefore, a data acquisition system with high resolution is necessary. Please also note the switching disturbance in both current and voltage waveforms at 20 kHz.

B. Tests at 50% SOC

As mentioned in Section V, two different tests are performed on the battery for analyzing the high- and low-frequency impedances of the battery. The first test used a WN perturbation with 2^{12} data points for identifying the impedance at frequencies higher than 100 Hz. The second test utilized a RN perturbation with 2^{16} data points, which was then used for analyzing the impedance in low-frequency region up to 100 Hz.

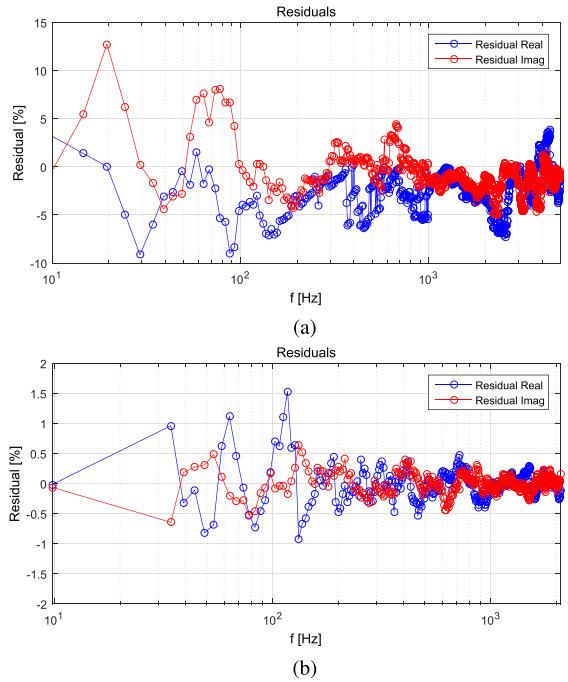

Fig. 8. Residual plots of KK analysis for the tests with the perturbation scale of (a) one and (b) four.

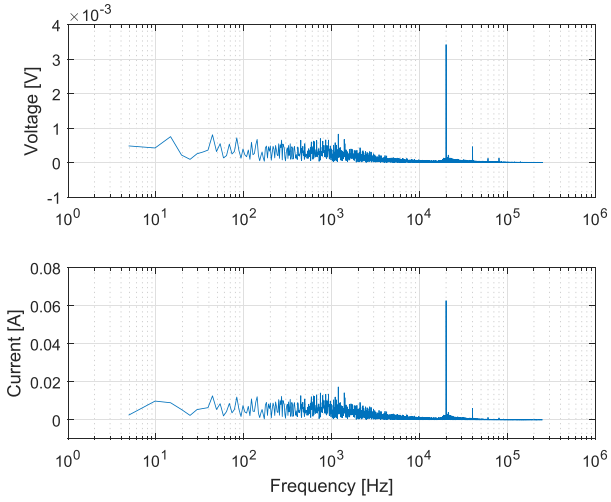

Fig. 9. Voltage and current waveforms during tests, where dc values are discarded.

For the test with WN perturbation, the cutoff frequency of moving average filter for the battery voltage is set to 100 Hz, since it is the lower limit for the frequency range of interest. On the other hand, the cutoff frequency for the RN test is chosen to be four times smaller for avoiding too much computational effort, since it is successfully able to remove the very low-frequency dynamics, which include the charging behavior of battery OCV.

Since most of battery estimation applications are based on the parameters of first semicircle on the Nyquist plots, it has been decided to perform the EIS down to a few hundred mHz, which is generally enough for determining the impedance of the first semicircle [5], [8]. Moreover, since the resolution of

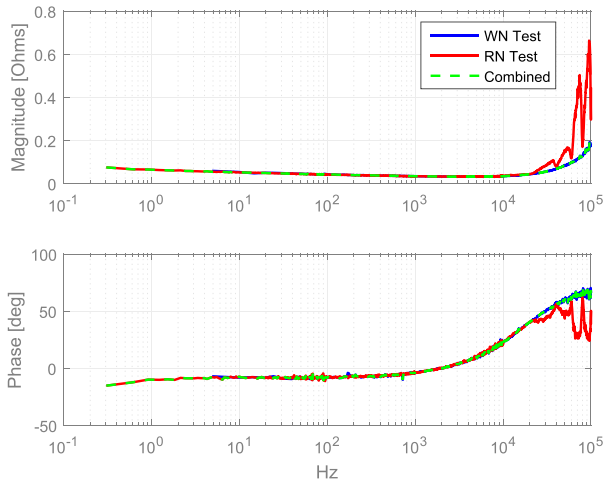

Fig. 10. Impedance spectra obtained by RN injected test (red), by WN injected test (blue), and the combination of both (green) at 50% SOC.

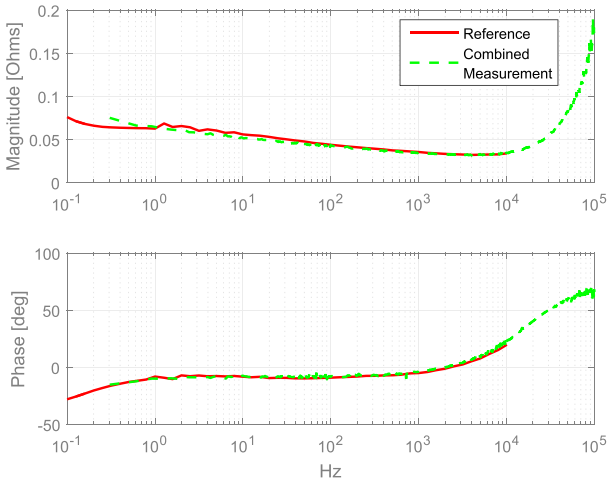

Fig. 11. Comparison of combined results with reference measurements at 50% SOC.

the frequency bandwidth is same with the lowest measured frequency, the frequencies far less than this level could cause a very big data set to deal with, which would in return result in a big computational effort. The results for tests at 50% SOC and the combined final result are presented in Fig. 10.

As it is anticipated, while the RN injection results in better results for low-frequency region, the high-frequency information is attenuated, resulting in an invalid measurement in the higher frequencies. In Fig. 11, the final obtained impedance information is compared with the reference measurement at 50% SOC.

The comparison of direct measurements (both measurements combined), the data fitted by equivalent-circuit model, and reference measurement are given in Fig. 12. As seen from this figure, the proposed method was able to measure the complex impedance of a battery with a high correlation with a commercially available high precision impedance analyzer over a wide frequency range. As seen from Fig. 12, there is a slight difference between two measurements in the order of milliohms. This result can be attributed to two reasons: 1) there are slight changes in the experimental setup, such as the cabling and the

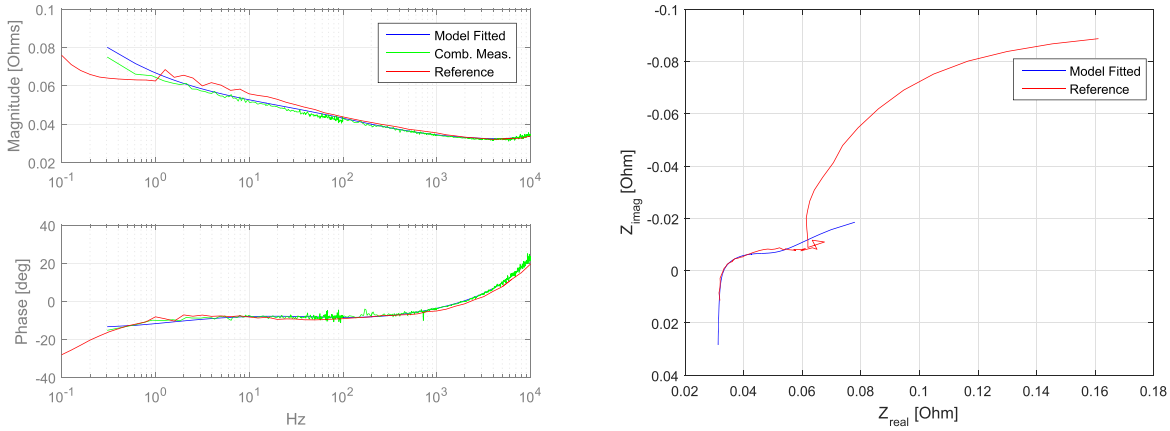

Fig. 12. Comparison of combined measurements (green curve), model fitted results (blue curve), and reference measurements (red curve) (a) presented as Bode diagram and (b) presented as Nyquist plot, where reference measurements are presented for a ranger of 10 mHz to 10 kHz and measurements with the offered method are between 0.3052 Hz and 20.4 kHz.

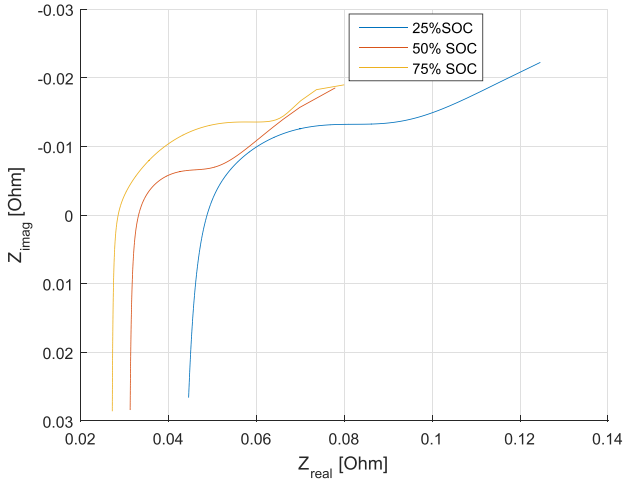

Fig. 13. Results for different SOC values.

TABLE I
EXTRACTED PARAMETERS FOR DIFFERENT SOC VALUES

Parameter	25% SOC	50% SOC	75% SOC
L_e $[\mu Henry]$	2.3139	2.2680	2.2580
R_e $[\Omega]$	0.0384	0.0306	0.0269
R_1 $[\Omega]$	0.2167	0.0160	0.0490
Q_1 $[F]$	13.2543	0.7656	1.5326
α_1	0.3704	0.6462	0.5974
χ $[\Omega/mm]$	0.13837	0.00352	0.00278
L_{BTS} $[mm]$	0.3191	254.9611	355.4115
r_{BTS} $[\Omega.mm]$	34.5956	1.4873	44.7483
q_{BTS} $[F/mm]$	4.2799	1.3945	0.6447
α_{BTS}	0.5776	0.8261	1.9803

environment, since Gamry EIS device includes temperature-controlled chamber with Faraday Cage; 2) it has been shown in the literature that batteries are electrochemical devices which are not in steady state. Even back-to-back tests of same batteries are expected to result in slightly different measurements due to small changes in SOC, system equilibrium, and temperature, etc. [37].

C. Tests at Various SOC Values

In this section, the battery was tested at three different SOC values, for confirming the capability of the proposed method. For each test, the battery was conditioned according to the EN 50342-1 CENELEC standard, as explained previously. The results for tests at 25%, 50%, and 85% SOC values are illustrated as Nyquist plots in Fig. 13. As it can be seen from the figure, quite a dramatic change in the impedance was observed depending on the SOC status of the battery. The behavior in the variation of the impedance curves are consistent with the previous findings in the literature [32], as the semicircles shift to the left direction in x-axis as the SOC increases.

In Table I, the extracted parameters after the model fitting for each tested SOC value is given. Extraction of these parameters are quite important since they could be used for battery status estimation by correct interpretation.

IX. CONCLUSION

This article contributes to the possibility of integrating sensitive EIS measurements of batteries within the capabilities of dc–dc converters. Since EIS measurements are the most powerful tool for identification and estimation of battery parameters, it is of great importance to be able to offer a cost-effective solution for performing online EIS measurements. Utilizing the proposed approach it would not be necessary to interrupt the operation of the power system to which the battery is connected.

The theoretical background is confirmed with an experimental setup consisting of an FPGA-controlled, boost converter-based battery charger connected to a 12-V, 7-Ah Yuasa NP7-12 lead-acid battery. The battery was tested at 25%, 50%, and 75% SOC values. As presented in the results, a good correlation between

the proposed method and commercially available EIS device was achieved using the method and proposed improvements.

Within the scope of the presented study, some improvements for the cross-correlation-based EIS measurement specific to batteries have been presented.

1) It has been proposed to perform moving average calculations on the battery current and voltage waveforms. This helps to remove the undesired dynamic effects caused by OCV variation as the battery is still under operation during the tests.
2) It has also been suggested to perform two different for low and high-frequency regions. For this purpose RN and WN injection on the duty cycle of the dc–dc converters have been utilized.
3) The preparation of noise signals and determination of noise perturbation magnitudes have also been addressed and demonstrated.
4) The postprocessing stage of the obtained data has been discussed. It has been demonstrated that utilization of even basic filters, such as moving averages and median filters, according to the fractional-decade processing are effective in smoothing out the results.
5) Even though the proposed approach is not a model-based technique, it has also been shown that curve fitting of the results according to the correct equivalent model enables further improvements of the results as well as parameter extraction for different applications such as SOC and SOH estimation.

The benefits of the proposed approach are as follows.

1) The proposed method scan all the frequencies in one go. Separate tests for each frequency of interest are not needed.
2) Testing time is relatively low since all frequencies are excited in one test.
3) It is not needed to disconnect the battery and interrupt the operation of the system since the approach is implemented within the capabilities of the dc–dc converter governing the battery.
4) The approach can be implemented at relatively lower costs compared to commercially available EIS instruments.

On the other hand, there are also a few challenges that need to be taken into consideration for implementing the proposed approach.

1) High resolution ADCs are needed, as the noise perturbation-caused voltage and current waveforms have quite small magnitudes.
2) Since the frequency resolution of the results depend on the total sampled data points, analyzing very low-frequencies (less than mHz range) would cause a lot of computational effort. This might be avoided by decreasing the sampling frequency with the cost of less precision at high-frequency impedance analysis.
3) The proposed approach is not able to focus on specific frequencies. In contrast to that, it scans all of the frequencies in a single test with a fixed resolution.
4) As the method is implemented for online applications, it should be considered that the testing time cannot be allowed to be too long since the state of batteries (such as SOC, SOH, or temperature) might vary during long test durations. Thus, these tests cannot reach μHz levels as the commercially available offline EIS devices, which keep the state of the battery controlled.
5) Being able to precisely control the duty cycle perturbation might be a challenge to some relatively slower digital controllers. Thus, the method is suggested to be implemented into the FPGAs, where the program is actually is being implemented as a hardware in the end.

ACKNOWLEDGMENT

The author would like to thank Assistant Prof. Dr. Deniz Yildirim, Department of Electrical Engineering, ITU, for providing NI DAQ instruments and Dr. Can Aksakal and Prof. Dr. Altug Sisman for providing the reference measurements that are taken at Inci GS Yuasa Laboratory in Energy Institute of Istanbul Technical University. This study has not been presented at a conference or submitted elsewhere previously.

REFERENCES

[1] F. Huet, "A review of impedance measurements for determination of the state-of-charge or state-of-health of secondary batteries," *J. Power Sources*, vol. 70, no. 1, pp. 59–69, 1998.

[2] P. Mauracher and E. Karden, "Dynamic modelling of lead/acid batteries using impedance spectroscopy for parameter identification," *J. Power Sources*, vol. 67, no. 1, pp. 69–84, 1997. [Online]. Available: http://www.sciencedirect.com/science/article/pii/S0378775397024981

[3] S. Rodrigues, N. Munichandraiah, and A. Shukla, "A review of state-of-charge indication of batteries by means of a.c. impedance measurements," *J. Power Sources*, vol. 87, no. 12, pp. 12–20, 2000.

[4] A. Hammouche, E. Karden, and R. W. D. Doncker, "Monitoring state-of-charge of Ni-MH and Ni-Cd batteries using impedance spectroscopy," *J. Power Sources*, vol. 127, no. 12, pp. 105–111, 2004, Eighth Ulmer Electrochemische Tage. [Online]. Available: http://www.sciencedirect.com/science/article/pii/S0378775303009443

[5] H. Blanke *et al.*, "Impedance measurements on lead–acid batteries for state-of-charge, state-of-health and cranking capability prognosis in electric and hybrid electric vehicles," *J. Power Sources*, vol. 144, no. 2, pp. 418–425, 2005. [Online]. Available: http://www.sciencedirect.com/science/article/pii/S0378775304011140

[6] J. Jespersen, A. Tnnesen, K. Nrregaard, L. Overgaard, and F. Elefsen, "Capacity measurements of Li-ion batteries using ac impedance spectroscopy," *World Electric Vehicle J.*, vol. 3, no. 1, pp. 127–133, 2009. [Online]. Available: http://www.mdpi.com/2032-6653/3/1/127

[7] Y. F. Luo, C. S. A. Gong, L. X. Chang, and Y. H. Liu, "AC impedance technique for dynamic and static state of charge analysis for Li-ion battery," in *Proc. IEEE Int. Symp. Consum. Electron.*, Jun. 2013, pp. 9–10.

[8] W. Waag, S. Kbitz, and D. U. Sauer, "Experimental investigation of the lithium-ion battery impedance characteristic at various conditions and aging states and its influence on the application," *Appl. Energy*, vol. 102, pp. 885–897, 2013, Special Issue on Advances in Sustainable Biofuel Production and Use – XIX International Symposium on Alcohol Fuels – ISAF. [Online]. Available: http://www.sciencedirect.com/science/article/pii/S030626191200671X

[9] D. I. Stroe, M. Swierczynski, A. I. Stan, V. Knap, R. Teodorescu, and S. J. Andreasen, "Diagnosis of lithium-ion batteries state-of-health based on electrochemical impedance spectroscopy technique," in *Proc. IEEE Energy Convers. Congr. Expo.*, Sep. 2014, pp. 4576–4582.

[10] J. Zhu, Z. Sun, X. Wei, and H. Dai, "A new lithium-ion battery internal temperature on-line estimate method based on electrochemical impedance spectroscopy measurement," *J. Power Sources*, vol. 274, pp. 990–1004, 2015. [Online]. Available: http://www.sciencedirect.com/science/article/pii/S0378775314018011

[11] A. Densmore and M. Hanif, "Determining battery SoC using electrochemical impedance spectroscopy and the extreme learning machine," in *Proc. IEEE 2nd Int. Future Energy Electron. Conf.*, Nov. 2015.

[12] T. Yokoshima *et al.*, "Impedance measurements of kilowatt-class lithium ion battery modules/cubicles in energy storage systems by square-current electrochemical impedance spectroscopy," *Electrochimica Acta*, vol. 246, pp. 800–811, 2017. [Online]. Available: http://www.sciencedirect.com/science/article/pii/S0013468617310721
[13] A. Waligo and P. Barendse, "A comparison of the different broadband impedance measurement techniques for lithium-ion batteries," in *Proc. IEEE Energy Convers. Congr. Expo.*, Sep. 2016.
[14] D. Depernet, O. Ba, and A. Berthon, "Online impedance spectroscopy of lead acid batteries for storage management of a standalone power plant," *J. Power Sources*, vol. 219, pp. 65–74, 2012. [Online]. Available: http://www.sciencedirect.com/science/article/pii/S0378775312011780
[15] W. Huang and J. Qahouq, "An online battery impedance measurement method using dc–dc power converter control," *IEEE Trans. Ind. Electron.*, vol. 61, no. 11, pp. 5987–5995, Nov. 2014.
[16] D. Howey, P. Mitcheson, V. Yufit, G. Offer, and N. Brandon, "Online measurement of battery impedance using motor controller excitation," *IEEE Trans. Veh. Technol.*, vol. 63, no. 6, pp. 2557–2566, Jul. 2014.
[17] R. Koch, R. Kuhn, I. Zilberman, and A. Jossen, "Electrochemical impedance spectroscopy for online battery monitoring - power electronics control," in *Proc. 16th Eur. Conf. Power Electron. Appl.*, Aug. 2014.
[18] Y.-D. Lee, S.-Y. Park, and S.-B. Han, "Online embedded impedance measurement using high-power battery charger," *IEEE Trans. Ind. Appl.*, vol. 51, no. 1, pp. 498–508, Jan. 2015.
[19] S. Moore and P. Barendse, "Online condition monitoring of lithium-ion batteries using impedance spectroscopy," in *Proc. IEEE Energy Convers. Congr. Expo.*, Oct. 2017, pp. 5617–5624.
[20] T. N. Gucin and L. Ovacik, "An impedance analyzer application using cross-correlation method," in *Proc. IEEE Int. Conf. Renewable Energy Res. Appl.*, Nov. 2016, pp. 265–269.
[21] B. Miao, R. Zane, and D. Maksimovic, "System identification of power converters with digital control through cross-correlation methods," *IEEE Trans. Power Electron.*, vol. 20, no. 5, pp. 1093–1099, Sep. 2005.
[22] J. Sawma, F. Khatounian, and E. Monmasson, "A modified cross-correlation method for the identification of systems with large bandwidth," in *Proc. 38th Annu. Conf. IEEE Ind. Electron. Soc.*, Oct. 2012, pp. 2121–2126.
[23] A. Barkley and E. Santi, "Improved online identification of a dc–dc converter and its control loop gain using cross-correlation methods," *IEEE Trans. Power Electron.*, vol. 24, no. 8, pp. 2021–2031, Aug. 2009.
[24] M. Shirazi, J. Morroni, A. Dolgov, R. Zane, and D. Maksimovic, "Integration of frequency response measurement capabilities in digital controllers for dc–dc converters," *IEEE Trans. Power Electron.*, vol. 23, no. 5, pp. 2524–2535, Sep. 2008.
[25] A. Barkley and E. Santi, "Online monitoring of network impedances using digital network analyzer techniques," in *Proc. 24th Annu. IEEE Appl. Power Electron. Conf. Expo.*, Feb. 2009, pp. 440–446.
[26] C. Pastor-Fernandez, W. D. Widanage, J. Marco, M.-A. Gama-Valdez, and G. H. Chouchelamane, "Identification and quantification of ageing mechanisms in lithium-ion batteries using the EIS technique," in *Proc. IEEE Transp. Electrific. Conf. Expo.*, Jun. 2016.
[27] C. Fleischer, W. Waag, H.-M. Heyn, and D. U. Sauer, "On-line adaptive battery impedance parameter and state estimation considering physical principles in reduced order equivalent circuit battery models: Part 1. Requirements, critical review of methods and modeling," *J. Power Sources*, vol. 260, pp. 276–291, 2014. [Online]. Available: http://www.sciencedirect.com/science/article/pii/S0378775314002249
[28] J. Bisquert, G. Garcia-Belmonte, P. Bueno, E. Longo, and L. Bulhes, "Impedance of constant phase element (CPE)-blocked diffusion in film electrodes," *J. Electroanalytical Chemistry*, vol. 452, no. 2, pp. 229–234, 1998. [Online]. Available: http://www.sciencedirect.com/science/article/pii/S0022072898001156
[29] A. V. Oppenheim and R. W. Schafer, *Discrete-Time Signal Processing*. Upper Saddle River, NJ, USA: Prentice Hall, 2010.
[30] A. B. Barkley, "Online identification, monitoring, and control of a dc/dc converter system using digital network analyzer techniques," Ph.D. dissertation, College Eng. Comput., Univ. South Carolina, South Carolina, USA, 2010.
[31] J. Ehlers, "Signal analysis concepts," Accessed on: May 11, 2018. [Online]. Available: http://www.technicalanalysis.org.uk/moving-averages/Ehle.pdf
[32] C. Aksakal and A. Sisman, "On the compatibility of electric equivalent circuit models for enhanced flooded lead acid batteries based on electrochemical impedance spectroscopy," *Energies*, vol. 11, no. 1, pp. 1–14, 2018.
[33] Use of transmission lines for electrochemical impedance spectroscopy, Gamry Instruments. Accessed on: Jun. 17, 2018. [Online]. Available: https://www.gamry.com/application-notes/EIS/use-of-transmission-lines-for-eis/
[34] J. Bisquert, "Influence of the boundaries in the impedance of porous film electrodes," *Phys. Chem. Chem. Phys.*, vol. 2, pp. 4185–4192, 2000. [Online]. Available: http://dx.doi.org/10.1039/B001708F
[35] B. A. Boukamp, "A linear Kronig-Kramers transform test for immittance data validation," *J. Electrochemical Soc.*, vol. 142, pp. 1885–1894, 1995.
[36] Lin-KK tool. IAM of Karlsruhe Institute of Technology. Accessed on: Jul. 13, 2019. [Online]. Available: https://www.iam.kit.edu/wet/english/Lin-KK.php
[37] J. P. Christophersen, C. G. Motloch, J. L. Morrison, I. B. Donnellan, and W. H. Morrison, "Impedance noise identification for state-of-health prognostics," in *Proc. 43rd Power Sources Conf.*, 2008.

Taha Nurettin Gücin was born on May 19, 1987, in Turkey. He received the B.Sc. degree in electrical engineering from Istanbul Technical University (ITU), in 2010, and the M.Sc. degree from ITU, Energy Institute, in 2013. He is currently working toward the Ph.D. degree with the Department of Electrical Engineering, ITU.

Between 2010 and 2017, he worked as a Research Assistant with ITU and Yalova University. Afterwards, he served as a Power Supply Engineer with Elettra Sincrotrone Elettra, Italy. His research interests cover the fields of power electronics, electrical machines and drives, electric vehicle technology, and renewable energy systems.

Levent Ovacik was born on May 13, 1964, in Edirne, Turkey. He received the B.Sc. and M.Sc. degrees in electrical engineering from Istanbul Technical University (ITU), Istanbul, Turkey, in 1985 and 1989, respectively, and the Ph.D. degree in electric power engineering from Rensselaer Polytechnic Institute (RPI), Troy, NY, USA, in 1998.

In May 1999, he joined the Department of Electrical Engineering, ITU, as an Assistant Professor. After his retirement in April 2018, he has been serving as a Consulting Engineer for electric equipment manufacturing industry. He is the Thesis Advisor of three doctoral students of the Graduate School of Science Engineering and Technology at ITU. His primary research interests include computational electromagnetics, design and optimization of magnetic devices, and power electronic converters for electromechanical power generation and energy storage systems.